Dyes and Pigments 133 (2016) 109–113

Contents lists available at ScienceDirect

Dyes and Pigments

journal homepage: www.elsevier.com/locate/dyepig

Synthesis and characterization of the copper doped Ca-La apatites

M.A. Pogosova [a, *], I.L. Kalachev [a], A.A. Eliseev [a], O.V. Magdysyuk [b], R.E. Dinnebier [b], M. Jansen [b], P.E. Kazin [a]

[a] Department of Chemistry, Moscow State University, 119991 Moscow, Russian Federation
[b] Max Planck Institute for Solid State Research, Heisenbergstrasse 1, 70569 Stuttgart, Germany

ARTICLE INFO

Article history:
Received 18 February 2016
Received in revised form
23 May 2016
Accepted 24 May 2016
Available online 27 May 2016

Keywords:
Apatite
Pigment
Copper
Color
Lanthanum

ABSTRACT

Copper-containing Ca-La hydroxyapatites (HAPs) with chemical compositions $Ca_{10-x}La_x(PO_4)_6O_2H_{1.5-x-y-\delta}Cu_y$ ($x = 0–1.79$; $y = 0–0.57$) were synthesized by solid state reaction. Structural parameters and atomic positions were refined using the Rietveld method in space group $P6_3/m$. It was found that La^{3+} ions occupied the Ca(2) position only and copper ions were located mainly inside the hexagonal channel. In contrast to known red-violet copper-doped Ca-apatites, the copper-doped Ca-La apatites exhibited lighter colors varying from pink to pale yellow and blue-grey tints. Chromophores in the compounds were characterized by diffuse reflectance spectroscopy, colorimetry, and resonant Raman spectroscopy.

1. Introduction

Apatite type phosphates with the general formula $M_{10}(PO_4)_6A_2$ (M – bivalent metal (Ca, Sr, Ba, Pb etc.) or monovalent-trivalent metal's mixture; A – OH or halogen) are widely used in different areas including medicine (bone implants, remedies) [1,2] and industrially as sorbents and catalysts [3–6]. They are of interest as materials for ion conductors [7] and luminophores [8,9]. An additional application for apatite-type compounds has been found recently: copper-doped apatites happened to exhibit bright colors [10,11] and one compound has been already produced as an inorganic pigment [12].

In connection with the high production volume of inorganic pigments with a wide range of colors the development of environmentally-friendly pigments is a vexing problem. Especially for yellow-orange pigments: contemporary inorganic dyes of this color range are mainly based on toxic lead and cadmium compounds. The recently developed brightly colored copper-doped alkaline-earth apatite-type phosphates have a general formula $M_{10}(PO_4)_6(Cu_xO_2H_{2-x-\delta})$ [10,11]. The copper ion substitutes hydrogen occupying position (0,0,0) inside the hexagonal channel and thus forming a linear monomer $[O\text{-}Cu\text{-}O]^{3-}$ or oligomer $[O\text{-}Cu_n\text{-}O_{n+1}]^{(n+2)-}$ anion (Fig. 1b) [10,11,13–16]. The color originates due to partial oxidation of Cu^+. Quite recently it has been shown that the color is produced by an unusual chromophore group — linear $[O\text{-}Cu\text{-}O]^-$ anion situated in the hexagonal channel [16].

Copper-doped calcium apatite exhibits 3 absorption bands: the main intense band **A** at 537 nm, a weak band **B** around 750 nm and a shoulder **C** at 450 nm [17]. **A** and **B** have been attributed to the main chromophore formed by the oxidized intrachannel copper ions. **C** has been assigned to an additional chromophore in trace quantities. Furthermore the relationship between relative intensity of the observed bands and the content of the copper ions points to the existence of one more absorption band which overlaps with **B** but has hypsochromically shifted maximum. The authors proposed that this band was also linked to the additional chromophore.

The wavelength of the main absorption band **A** depends on the nature of the alkaline-earth metal M: 595 nm for Ba, 565 nm for Sr, and 537 nm for Ca [10,11,14]. Therefore, the rise of the cation size (and decrease of the cation field strength) leads to the regular bathochromic shift of the band. Hence, one might suggest that the use of a smaller-size cation or a cation with higher charge may change the red-violet (magenta) color of copper-doped calcium hydroxyapatite (Ca-HAP) to one in the red-orange-yellow range.

* Corresponding author. Tel.: +7 (495) 939 34 40.
E-mail addresses: pogosova.m.a@yandex.ru (M.A. Pogosova), martefyo@gmail.com (I.L. Kalachev), eliseev@inorg.chem.msu.ru (A.A. Eliseev), oxana.magdysyuk@diamond.ac.uk (O.V. Magdysyuk), r.dinnebier@fkf.mpg.de (R.E. Dinnebier), m.jansen@fkf.mpg.de (M. Jansen), kazin@inorg.chem.msu.ru (P.E. Kazin).

http://dx.doi.org/10.1016/j.dyepig.2016.05.044
0143-7208/

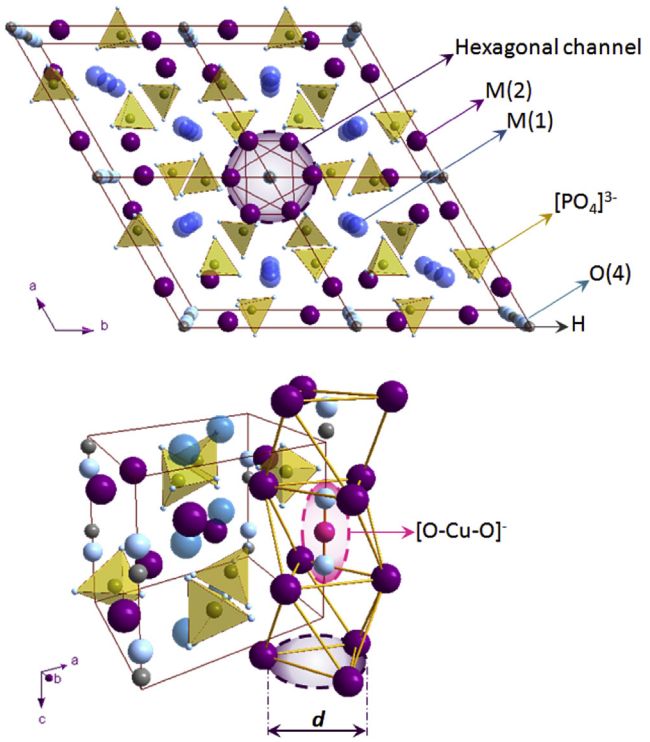

Fig. 1. Crystal structure of the hydroxyapatite (a.) and the position of the main chromophore, intrachannel linear anion $[O\text{-}Cu\text{-}O]^-$ (b.).

However, recently reported results show that the partial substitution of Ca influences the color in another way. The substitution by trivalent cations Y^{3+} and Bi^{3+} causes the disappearance of the initial magenta color [18,19]. Both of the cations occupy only the Ca(2) position, which form the wall of the hexagonal channels (Fig. 1). Intrachannel copper ions are situated quite close to Ca(2) position (Fig. 1b). Hence, yttrium and bismuth ions may strongly influence the chromophore $[O\text{-}Cu\text{-}O]^-$. The substitution of Bi for Ca suppresses the chromophore by simultaneous (i) limiting the copper introduction into the channel and (ii) hindering the oxidation of colorless $[O\text{-}Cu\text{-}O]^{3-}$ to chromophore $[O\text{-}Cu\text{-}O]^-$ [18]. Both effects are apparently linked to more covalent nature of $Bi^{3+}(2)—O^{2-}$ (4) bond in comparison with $Ca^{2+}(2)—OH^-$ (4). The electron density is shifted towards Bi^{3+} from the OCuO-group thus destabilizing the latter, especially if copper is in high oxidation state. While the initial chromophore disappears on the doping, another type of chromophore which is formed by copper ions in Ca(1)/Ca(2) positions arises [18]. This chromophore adds the yellow color component and changes the original magenta color of Cu-doped Ca-HAP to the sand-yellow color of Cu-doped Ca-Bi-HAP.

Lanthanum cation La^{3+} has the same size and charge as Bi^{3+} and may have a similar influence on the behavior of the chromophore. However, in contrast to bismuth, La^{3+} has no lone electron pair, so the $La^{3+}(2)—O^{2-}$ (4) bond may be less covalent than $Bi^{3+}(2)—O^{2-}$ (4) and one may consider that La-for-Ca substitution would not impede the introduction of copper ions in the channel to such extent as the Bi-for-Ca substitution does. In this paper, we describe results on synthesis and study of such copper-doped Ca-La-HAPs.

2. Experimental

Chemical grade $CaCO_3$, $(NH_4)_2HPO_4$, $La(NO_3)_3\cdot 6H_2O$ and CuO were used for solid state synthesis of three types of compounds: lanthanum-doped (La-for-Ca substituted), copper-doped (Cu-for-H substituted), and lanthanum-and-copper-doped. $La(NO_3)_3\cdot 6H_2O$ was previously annealed at 850 °C for 2 h and decomposed to La_2O_3 which was used for the main synthesis. The general formulas of obtained compounds is $Ca_{10-x0}La_{x0}(PO_4)_6O_2H_{2-x0-y0-\delta}Cu_{y0}$ where $x_0 = 0, 0.5, 1, 2$ and $y_0 = 0, 0.2, 0.6$. As it is known that the Cu-for-Ca substitution in Cu-doped Ca-Bi-HAP leads to a yellow chromophore formation [18], in order to increase quantity of this possible chromophore the additional samples with small cation deficiency were prepared: $(Ca_9La)_{0.99}(PO_4)_6O_2H_{2-x-y-\delta}Cu_y$ where $y_0 = 0, 0.2, 0.6$. Indexes x_0 and y_0 represent nominal compositions. These compounds further will be denoted as $\mathbf{Lx_0C10y_0}$ for cation-stoichiometric and $\mathbf{L99C10y_0}$ for cation-deficient series. All samples were obtained by solid state synthesis according to the next method: reagents were mixed in stoichiometric proportions in quantities to obtain ca. 2 g of the final compound and ground in an agate mortar. The obtained powders were annealed in a muffle furnace at 600 °C (heating for 1 h, holding for 1 h) and then at 800 °C (heating for 1 h, holding for 3 h) with subsequent grinding in an agate mortar. This step provided decomposition of calcium carbonate and ammonium hydrophosphate to calcium phosphates without the loss of phosphorus. The powders obtained after the first step were annealed twice at 1150 °C (heating for 1.5 h, holding for 5 h, air quenching) with intermediate regrinding in an agate mortar. Then the powders were pressed into pellets and annealed at 1150 °C (heating for 1.5 h, holding for 5 h). The annealing was carried out twice with air quenching. After the second anneal the pellets were grinded into a powder.

PXRD patterns for all target samples were registered using a Rigaku D/Max-2500 diffractometer (with CuK_α radiation and 2θ range from 5 to 80°, step = 0.02°). X-Ray diffraction was used after each step of synthesis to control the phase composition of the samples. PXRD patterns with high intensity exceeding 10^5 counts were additionally registered for selected samples on Bruker-AXS D8 (with $CuK_{\alpha 1}$ radiation and 2θ range from 10 to 120°, step = 0.01°). Crystal structure of obtained compounds were refined by the Rietveld method in space group $P6_3/m$ using the JANA 2006 software [20] with refined parameters analogical to those described in Ref. [18]: unit cell dimensions; atomic positions (except hydrogen; O(4) was refined at the (0,0,*z*) split position) and atomic displacement parameters; calcium and lanthanum occupancies at M(2) position; copper occupancies at (0,0,0) position. Estimated values for *x* and *y* of $Ca_{10-x}Bi_x(PO_4)_6O_2H_{2-x-y-\delta}Cu_y$ were considered using the refined occupancies. Raman spectra were registered on a RENISHAW in Via Reflex (scanning range = 100–1500 cm^{-1}, λ = 514 nm). The color of the target samples was characterized using diffuse reflectance spectroscopy recorded on the Perkin Elmer Lambda 950 spectrometer (13 cm integrating sphere with SPECTRALON top-coating, scanning range: from 200 to 1200 nm, scanning step = 1 nm). Colorimetric measurements in CIE $L^*a^*b^*$ color space were provided using reflex camera Olympus e-420 (5400 K illuminant; ISO = 200; lightroom with length-width-depth = 35 cm-25 cm-32 cm) and the PhotoImpact 12 software [18].

3. Results and discussion

3.1. Details of the crystal structure

The hydroxyapatite crystal structure is shown in Fig. 1. Selected results of Rietveld refinement are presented in Table 1. Diffraction patterns and further crystallographic data are shown in Fig. 2 and in the Supplementary Information, Figs. A1–A12, Tables A1–A12. All the samples represent apatite as a major phase. Some samples contain admixtures: calcium and/or lanthanum phosphates with mass fraction below 12%. The unit cell parameters, nominal and

Table 1
Results of the Rietweld refinement of PXRD patterns for the samples $Ca_{10-x}La_x(PO_4)_6O_2H_{2-y-\delta}Cu_y$: x and y — content of lanthanum and copper respectively determined by the atomic occupancy refinement; a and c — unit cell parameters; V — unit cell volume; d — diameter of the hexagonal channel.

Sample	Color	x_0	y_0	R_{wp}	R_p	RF_{all}	GOF	a, Å	c, Å	V, Å^3	x	y	d, Å	By-phases, mass. %
L0C0[a]	White		0	5.51		1.67	1.28	9.4149(1)	6.8789(1)	528.06(1)	–	–	4.705(1)	–
L0C2	Light-magenta		0.2	8.11	6.27	2.62	1.79	9.4222(1)	6.8873(1)	529.53(1)	–	0.21(1)	4.718(1)	–
L0C6	Magenta		0.6	7.78	5.75	2.80	1.69	9.4317(1)	6.9080(1)	532.12(1)	–	0.57(1)	4.745(1)	–
L05C0	White	0.5	0	10.02	7.34	2.95	1.55	9.4394(2)	6.8895(2)	531.62(2)	0.44(1)	–	4.604(1)	0.6 La_3PO_7
L05C2	Pink	0.5	0.2	8.45	6.37	2.57	1.06	9.4519(3)	6.9169(2)	535.16(3)	0.51(1)	0.24(1)	4.693(1)	11.7 $Ca_3(PO_4)_2$ 1.1 $LaPO_4$
L05C6	Violet-brick-red	0.5	0.6	7.38	5.66	3.01	1.02	9.4553(3)	6.9229(2)	536.00(3)	0.48(1)	0.37(1)	4.678(1)	3.1 $Ca_3(PO_4)_2$
L99C0	White	0.99	0	4.45	3.12	3.86	1.53	9.4313(2)	6.8954(2)	531.17(2)	0.55(1)	–	4.492(1)	0.7 La_3PO_7
L99C2	Sand-yellow	0.99	0.2	9.18	7.03	2.66	1.08	9.4646(3)	6.9213(3)	536.93(4)	0.75(1)	0.24(1)	4.582(1)	6.2 $Ca_3(PO_4)_2$ 2.9 $LaPO_4$
L99C6	Chaki	0.99	0.6	8.01	6.27	3.44	1.10	9.4687(3)	6.9274(2)	537.87(3)	0.83(1)	0.31(1)	4.613(1)	3.9 $LaPO_4$
L1C0[a)]	White	1	0	3.63		1.53	2.34	9.4447(3)	6.9028(3)	533.25(3)	0.78(3)	–	4.487(2)	–
L1C2	Pale pink	1	0.2	8.79	6.68	2.24	1.38	9.4512(3)	6.9078(2)	534.38(3)	0.78(1)	0.23(1)	4.509(1)	1.5 La_3PO_7
L1C6	Cold pink	1	0.6	6.03	4.56	2.27	1.02	9.4620(1)	6.9230(1)	536.78(1)	0.92(1)	0.46(1)	4.518(1)	–
L2C0[a]	White	2	0	2.40		1.41	1.72	9.4610(1)	6.9194(1)	536.37(1)	1.45(2)	–	4.372(1)	5.7 $LaPO_4$
L2C2	Pale grey	2	0.2	7.04	5.27	2.03	1.23	9.4614(1)	6.9230(1)	536.71(1)	1.48(1)	0.15(1)	4.374(1)	4.1 La_3PO_7 3.4 $LaPO_4$
L2C6	Pale blue	2	0.6	2.83	1.93	2.42	2.14	9.4625(1)	6.9324(1)	537.56(1)	1.79(1)	0.17(1)	4.341(1)	1.7 $LaPO_4$

[a] Data are taken (or calculated) from Ref. [25].

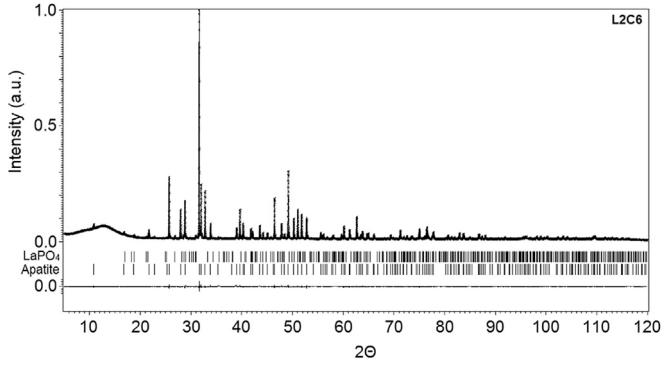

Fig. 2. Experimental, refined and differential PXRD patterns for **L2C6**.

established content of lanthanum (x_0 and x respectively) and copper (y_0 and y respectively) and diameter d (specified as double distance between M(2) and (0,0,0.25) position, see Fig. 1) of the hexagonal channel will be discussed. Crystal structure data of copper-free samples **L0C0**, **L1C0**, and **L2C0** were published in our earlier paper [25].

3.1.1. *Lanthanum-doped samples* – ***LxC0***

The lanthanum ions occupy the Ca(2) position only [25]. The La-for-Ca substitution leads to the increase of unit cell volume V (see Table 1) in accord with the larger size of the La^{3+} ion in comparison with Ca^{2+} ($R_{La3+} = 1.03$ Å, $R_{Ca2+} = 1.00$ Å, coordination number = 6 [21]). However La^{3+}-for-Ca^{2+} substitution is accompanied by the decrease of the diameter d of the channels. This is connected with synchronous O^{2-}-for-OH^- substitution inside the channel resulting in the stronger Coulomb interaction which provides decrease of the M(2)—O^{2-}(4) distance and therefore d [18,25].

3.1.2. *Copper-doped samples* – ***L0Cy***

Copper ions occupy only the intrachannel position at (0,0,0) in accord with previous data [10,11,13] designating the Cu-for-H substitution according to reaction:

$$4\,CuO + 12\,(OH)^- \rightarrow 4\,[O\text{-}Cu\text{-}O]^{3-} + 4\,\{vacancy\} + 6H_2O\uparrow + O_2\uparrow$$

The increase of the V and d caused by the copper injection into the hexagonal channel was described in Refs. [10,11] in detail. Here it should be mentioned that these changes are expected because of the larger size of the copper ion in comparison with hydrogen ion of intrachannel OH^- anion.

3.1.3. *Lanthanum- and copper-doped samples* – ***LxCy***

The copper ions occupy the (0,0,0) position inside the channel in the same way as in the lanthanum-free samples. Content of intrachannel copper y estimated by the refinement of the site occupancy is close to nominal values for **Lx_0C2** samples and a factor of 1.5–3 lower than nominal one for **Lx_0C6** samples (Table 1). In **L2C6**, y is 0.17, and the estimated from the site occupancy La-content x is of 1.79 so that the charge balance yields allowable maximum of $y = 0.21$. Therefore combined La^{3+} for Ca^{2+}-and-H^+ and $Cu^{(1+\delta)+}$ for H^+ substitution removes practically all hydrogen atoms from the structure. Therefore copper is able to substitute the remaining hydrogen even at high La content in contrast to the Bi-doped compounds in which approximately at the same Bi for Ca substitution degree, copper is practically absent in the channels [18]. Incorporation of copper is accompanied by the V and d increase similar to that in lanthanum-free apatites.

3.2. *Spectroscopic methods*

Diffuse reflectance spectra for **L0C2**, **L05C2**, **L99C2**, **L1C2** and **L2C2** are presented in Fig. 3. Lanthanum-free sample **L0C2** has the same spectrum as the copper-doped calcium apatite described in

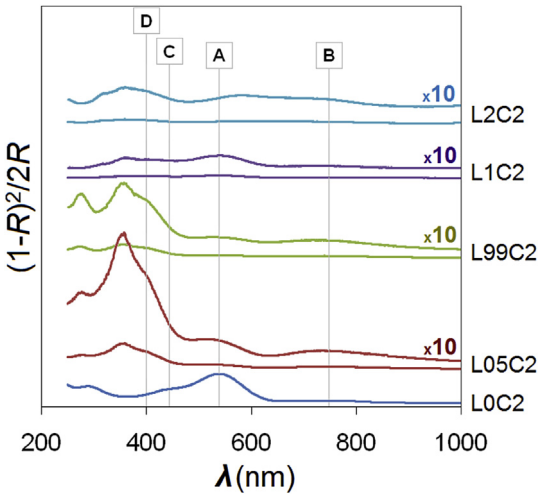

Fig. 3. Diffuse reflectance spectra for **L0C2**, **L05C2**, **L99C2**, **L1C2** and **L2C2**.

Refs. [11,14,18] and reveals the intense band **A**, the weak band **B** and the middle-intensity shoulder **C**. With La-for-Ca substitution, an additional middle-intensity absorption band **D** at 400 nm emerges. According to Fig. 3, with the *x* growth to 0.5 the intensity of **A** severely decreases while the position of **A** stays the same. The intensity of **C** also decreases during the *x* growth. It is difficult to analyze the change of the **C** position because of its low intensity and the presence of the shoulder of the **D** band. The absorption in the vicinity of **B** is present in all the samples.

Raman spectra of **L0C2**, **L05C2**, **L99C2**, **L1C2** and **L2C2** are presented in Fig. 4. All the spectra contain bands of the $[PO_4]^{3-}$ group which are similar to those described in Refs. [18,22,23]. The band **La2** at 511 ± 1 cm^{-1} observed in all lanthanum-doped samples can be assigned to La(2)—O(4) stretching mode, according to [24,25]. Lanthanum-free copper-doped sample **L0C2** represents the intense resonant band **Cu0** at 650 cm^{-1} and its overtone **O-Cu0** at 1300 cm^{-1}. The intensity of these bands gradually decreases with the *x* growth, up to full absence in **L1C2**. La-for-Ca substitution causes an additional band to emerge at 595 cm^{-1} (**Cu1**) with the overtone at 1187–1189 cm^{-1} (**O-Cu1**) suggesting its resonant character. The *x* growth is accompanied by the increase of the **Cu1** intensity.

3.3. Relations between crystallographic, spectral and colorimetry data

As mentioned in the introduction the main absorption band **A** providing the magenta color of the samples is related to the oxidized intrachannel copper ions, namely to the $[O\text{-}Cu\text{-}O]^{-}$-anion. This magenta chromophore will be further denoted as “M-chromophore”. It has been also shown that the intrachannel copper(I) doesn’t impart any color and the intensity of **A** correlates with the quantity of the oxidized copper situated in the channel, which represents only a fraction of all intrachannel copper; the intensity of **A** usually increases with the overall copper quantity at the same preparation conditions [11,14].

As described in Refs. [16,18], the M-chromophore showed the resonant band at 650 cm^{-1} with overtones in the Raman spectra. In our work, the same resonant band denoted as **Cu0** with the first overtone is observed (see Fig. 4), its intensity correlating with the intensity of **A**. Therefore the existence of M-chromophore is additionally confirmed by the presence of the resonant band **Cu0**.

In Refs. [14], it was mentioned that the intensity of **B** and **C** depended on the copper content stronger than the intensity of **A** suggesting that **B** and **C** were caused by the simultaneous presence of two copper ions at two close but different positions: intrachannel and Ca(2) (Fig. 1). It was proposed that such Cu-for-Ca substitution could be initiated by the local deformation of hexagonal channels by the intrachannel copper ions. The combination of **B** (blue) and **C** (yellow) absorption bands leads to the emergence of a green color (which is characteristic for copper compounds with d-d transitions) [17]. Therefore the chromophore which causes the **B** and **C** formation will be further denoted as “G-chromophore”.

The observed **D** absorption band is analogous to known **D**-band located at 400 nm in Bi-for-Ca substituted copper-doped calcium hydroxyapatites [18]. This **D**-band was assigned to the chromophore which was formed by copper ions Cu^{2+} localized in Ca-sites and this Cu-for-Ca substitution was apparently activated by the Bi-for-Ca substitution which deformed the hexagonal channel decreasing its average diameter.

The La-for-Ca substitution leads to a similar narrowing of the hexagonal channel (Table 1) and forces the **D**-band to emerge in the copper-doped samples. The absorption band **D** adds the yellow color to the samples. Thus this yellow chromophore will be further considered as the “Y-chromophore”. This chromophore is connected to Cu substituting Ca in a very small amount [18], hence only a small fraction of copper is involved (corresponding to *y* of 0.03 or less), therefore an intrachannel copper content may remain close to a nominal one.

In copper-doped Bi-for-Ca substituted apatites, the resonant band at 593 cm^{-1} in the Raman spectrum was related to the **D**-band [18]. Thus the equivalent resonant band **Cu1** at 595 cm^{-1} observed in our Cu-doped La-for-Ca substituted compounds (see Fig. 4) can be attributed to the Y-chromophore.

It should be mentioned that in the UV-VIS spectra of **L1C1** and **L2C2**, a small absorption is observed in the vicinity of band **A** while no resonant band at about 650 cm^{-1} is found in the corresponding Raman spectra. These samples apparently contain additional unidentified chromophores located either in the apatite compound or in an admixture phase.

Chromatic coordinates a^* and b^* for **L0C2**, **L05C2**, **L99C2**, **L1C2** and **L2C2** are presented in Fig. 5 (numeric values of L^*, a^* and b^* are presented in Table A13). Introduction of lanthanum causes the irregular color change of copper-doped calcium hydroxyapatites: magenta, pink, sand-yellow, pale pink, pale grey for **L0C2**, **L05C2**, **L99C2**, **L1C2**, **L2C2** respectively. To discuss this color variation it is

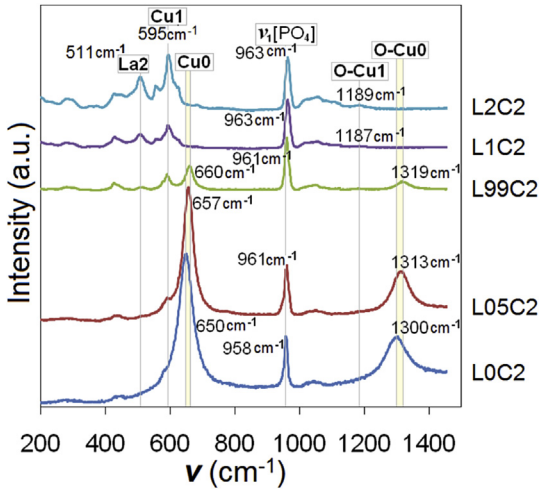

Fig. 4. Raman spectra for **L0C2**, **L05C2**, **L99C2**, **L1C2** and **L2C2**.

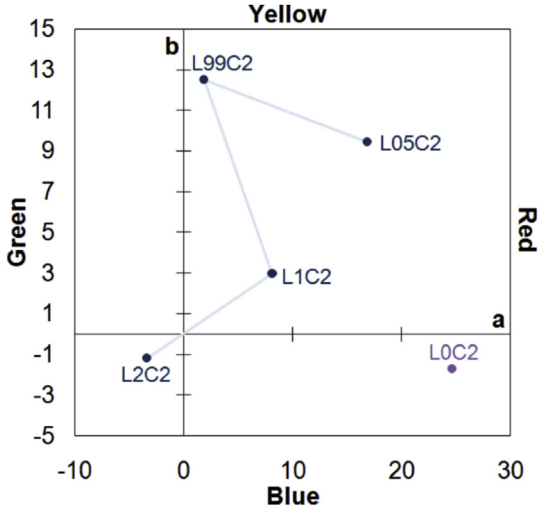

Fig. 5. Chromatic coordinates a^* and b^* for **L0C2**, **L05C2**, **L99C2**, **L1C2** and **L2C2**.

conveniently to distinguish the lanthanum substitution impact to each of the chromophores.

1) Increase of the La-content *x* causes a gradual suppression of M-chromophore characterized by the **A** and **Cu0** bands. The **L2C2** compound shows full absence of **A** and **Cu0** but contains a distinct amount of intrachannel copper ($y = 0.15$). The absence of M-chromophore implies the absence of intrachannel $[O\text{-}Cu\text{-}O]^{-}$, i.e. all the intrachannel copper is in a low oxidation state, presumably +1. The destabilization of the intrachannel copper higher oxidation state may be caused by the shift of electron density from intrachannel $O^{2-}(4)$ towards $La^{3+}(2)$ on the La for Ca substitution (as was proposed for corresponding bismuth-containing samples [18]).

2) Increase of *x* promotes the Cu-for-Ca substitution and Y-chromophore formation characterized by the **D** and **Cu1** bands. The cation-deficient sample **L99C2** shows the highest content of Y-chromophore as a lack of Ca obviously facilitates the Cu-for-Ca substitution.

3) As the absorption in the vicinity of **B-**band is observed in all samples, we may assume that the G-chromophore persists on the La-for-Ca substitution. As far as copper-ions are found in the hexagonal channels in considerable amount in all the compounds, the presence of G-chromophore is in line with the earlier assumption [17] that this chromophore arises due to the presence of the intrachannel copper ions and the adjacent Cu-for-Ca substitution. In the corresponding Cu-doped Bi-for-Ca substituted apatites [18], the practical absence of G-chromophore may be then explained by the fact that on this substitution the copper-ions are expelled from the channels.

Therefore, moving from **L0C2** to **L05C2** we see the color becomes pale due to a decrease of the M-chromophore and shifts to a red tint due to a contribution from Y-chromophore. The prevailing Y-chromophore provides a sand-yellow color of **L99C2**. The color brightness is somewhat suppressed due to contribution from G- and M-chromophores though. Dull colors of **L1C2** and **L2C2** are caused by the presence of both Y- and G-chromophores and unidentified chromophores as well.

4. Conclusions

La-for-Ca substitution in the copper-doped HAPs leads to the lanthanum introduction into the Ca(2) position only. This is accompanied by a minor extrusion of copper ions out of the channel and prevents the oxidation of the remaining intrachannel copper(I) so that the main M-chromophore $[O\text{-}Cu\text{-}O]^{-}$ formation is suppressed. Simultaneously a new Y-chromophore emerges which is characterized by the absorption band at 400 nm and resonant Raman band at 591–595 cm^{-1} and is assigned to oxidized copper ions at calcium positions by analogy with that in copper-doped Ca-Bi-HAPs, described in Ref. [18]. Thus the La-for-Ca substitution leads to the color change from intense magenta (red-violet) to yellow tint. In comparison with the copper-doped Ca-Bi-HAPs, the color is paler due to the lower content of the Y-chromophore.

Acknowledgements

The work was supported by Russian Foundation for Basic Research(RFBR), grant 14-03-00643-a.

Appendix A. Supplementary data

Supplementary data related to this article can be found at http://dx.doi.org/10.1016/j.dyepig.2016.05.044.

References

[1] Low HR, Phonthammachai N, Maignan A, Stewart GA, Bastow TJ, Ma LL, et al. The crystal chemistry of ferric oxyhydroxyapatite. Inorg Chem 2008;47:11774–82.
[2] Nassif N, Martineau F, Syzgantseva O, Gobeaux F, Willinger M, Coradin T, et al. In vivo inspired conditions to synthesize biomimetic hydroxyapatite. Chem Mater 2010;22:3653–63.
[3] Srinivasan M, Oferraris C, White T. Cadmium and lead ion capture with three dimensionally ordered macroporous hydroxyapatite. Environ Sci Technol 2006;40:7054–9.
[4] Xu Y, Schwartr FW. Sorption of Zn^{2+} and Cd^{2+} on hydroxyapatite surfaces. Environ Sci Technol 1994;28:1472–80.
[5] Meski S, Ziani S, Khireddine H. Removal of lead ions by hydroxyapatite prepared from the egg shell. J Chem Eng 2010;55:3923–8.
[6] Sugiyama S, Minami T, Moriga T, Hayashi H, Moffat JB. Calcium–lead hydroxyapatites: thermal and structural properties and the oxidation of methane. J Solid State Chem 1998;135:86–95.
[7] Jacobson AJ. Materials for solid oxide fuel cells. Chem Mater 2010;22:660–74.
[8] Al-Kattana A, Girod-Fullanaa S, Charvillat C, Ternet-Fontebassoa H, Dufoura P, Dexpert-Ghysb J, et al. Biomimetic nanocrystalline apatites: emerging perspectives in cancer diagnosis and treatment. Int J Pharm 2012;423:26–36.
[9] Piriou B, Fahmi D, Dexpert-Ghys J, Taitai A, Lacout JL. Unusual fluorescent properties of Eu 3+ in oxyapatites. J luminescence 1987;39:97–103.
[10] Kazin PE, Karpov AS, Jansen M, Nuss J, Tretyakov YD. Crystal structure and properties of strontium phosphate apatite with oxocuprate ions in hexagonal channels. Z Anorg Allg Chem 2003;629:344–52.
[11] Karpov AS, Nuss J, Jansen M, Kazin PE, Tretyakov YD. Synthesis, crystal structure and properties of calcium and barium hydroxyapatites containing copper ions in hexagonal channels. Solid State Sci 2003;5:1277–83.
[12] Pigment 28–5333 PK. http://www.ferro.com/NR/rdonlyres/9481A00D-F9FD-4B0D-B4CD-1F6D2AE7223A/0/PS03Inorganic_Pigments_For_Artist_Colours.pdf; April 17th, 2016.
[13] Pogosova MA, Kazin PE, Tretyakov YD. Synthesis and characterisation of copper doped Ca–Li hydroxyapatite. Nucl Instrum Methods Phys Res B 2012;284:33–5.
[14] Kazin PE, Zykin MA, Tretyakov YD, Jansen M. Synthesis and properties of colored copper-containing apatites of composition $Ca5(PO4)3Cu_YO_{Y+d}(OH)_{0.5-Y-d}X_{0.5}$ (X = OH, F, Cl). Russ J Inorg Chem 2008;53:362–6.
[15] Kazin PE, Zykin MA, Romashov AA, Tretyakov YD, Jansen M. Synthesis and properties of colored copper-containing alkaline-earth phosphates with an apatite structure. Russ J Inorg Chem 2010;55:145–9.
[16] Kazin PE, Zykin MA, Zubavichus YV, Magdysyuk OV, Dinnebier RE, Janzen M. Identification of the chromophore in the apatite pigment $[Sr_{10}(PO_4)_6(Cu_xOH_{1-x-y})_2]$: linear OCuO_ featuring a resonance Raman effect, an extreme magnetic anisotropy, and slow spin relaxation. Chem Eur J 2014;20:165–78.
[17] Kazin PE, Zykin MA, Tret'yakov YD, Jansen M. Synthesis and properties of colored copper-containing apatites of composition Ca 5 (PO 4) 3 Cu y O y+ δ (OH) 0.5− y− δ X 0.5 (X= OH, F, Cl). Russ J Inorg Chem 2008;53:362–6.
[18] Pogosova MA, Provotorov DI, Eliseev AA, Kazin PE, Jansen M. Synthesis and characterization of the Bi-for-Ca substituted copper-based apatite pigments. Dyes Pigment 2015;113:96–101.
[19] Pogosova MA, Kazin PE, Tretyakov Yu D, Jansen M. Synthesis, structural features, and color of calcium-yttrium hydroxyapatite with copper ions in hexagonal channels. Russ J Inorg Chem 2013;58:381–6.
[20] Petříček V, Dušek M, Palatinus L. Crystallographic computing system JANA2006: general features. Z für Kristallogr Mater 2014;229:345–52.
[21] Shannon RD. Revised effective ionic radii and systematic studies of interatomic distances in halides and chalcogenides. Acta Crystallogr Sect A Cryst Phys Diffr Theor General Crystallogr 1976;32:751–67.
[22] Tmar Trabelsi I, Madani A, Mercier AM, Toumi M. Rietveld refinement and ionic conductivity of $Ca_{8.4}Bi_{1.6}(PO_4)_6O_{1.8}$. J Solid State Chem 2013;197:154–9.
[23] de Aza PN, Guitian F, Santos C. Vibrational properties of calcium phosphate compounds. 2. Comparison between hydroxyapatite and b-tricalcium phosphate. J Chem Mater 1997;9:916–22.
[24] Serret A, Cabanas MV, Vallet-Regi M. Stabilization of calcium oxyapatites with lanthanum (III)-created anionic vacancies. Chem Mater 2000;12:3836–41.
[25] Kazin PE, Pogosova MA, Trusov LA, Kolesnik IV, Magdysyuk OV, Dinnebier RE. Crystal structure details of La- and Bi-substituted hydroxyapatites: evidence for LaO+ and BiO+ with a very short metal-oxygen bond. Paper is submitted to the Journal of Solid State Chemistry.